



HAL
open science

Photoreduction of CO₂ to CH₄ over Efficient Z-Scheme γ -Fe₂O₃/g-C₃N₄ Composites

Thanh-Binh Nguyen, Thuy Hang Dinh Thi, Doan Pham Minh, Hien Bui Minh, Ngoc Quynh Nguyen Thi, Bang Nguyen Dinh

► To cite this version:

Thanh-Binh Nguyen, Thuy Hang Dinh Thi, Doan Pham Minh, Hien Bui Minh, Ngoc Quynh Nguyen Thi, et al.. Photoreduction of CO₂ to CH₄ over Efficient Z-Scheme γ -Fe₂O₃/g-C₃N₄ Composites. Journal of Analytical Methods in Chemistry, 2022, 2022, pp.1358437. 10.1155/2022/1358437. hal-03659641

HAL Id: hal-03659641

<https://imt-mines-albi.hal.science/hal-03659641>

Submitted on 5 May 2022

HAL is a multi-disciplinary open access archive for the deposit and dissemination of scientific research documents, whether they are published or not. The documents may come from teaching and research institutions in France or abroad, or from public or private research centers.

L'archive ouverte pluridisciplinaire **HAL**, est destinée au dépôt et à la diffusion de documents scientifiques de niveau recherche, publiés ou non, émanant des établissements d'enseignement et de recherche français ou étrangers, des laboratoires publics ou privés.



Distributed under a Creative Commons Attribution 4.0 International License

Research Article

Photoreduction of CO₂ to CH₄ over Efficient Z-Scheme γ -Fe₂O₃/g-C₃N₄ Composites

Thanh-Binh Nguyen ¹, Thuy Hang Dinh Thi,^{1,2} Doan Pham Minh ³, Hien Bui Minh,¹
Ngoc Quynh Nguyen Thi,⁴ and Bang Nguyen Dinh¹

¹VNU University of Science, Hanoi, Vietnam

²Vietnam Maritime University, 484 Lach Tray, Hai Phong, Vietnam

³IMT Mines Albi, Campus Jarlard, Albi CT Cedex 09 81013, Albi, France

⁴Vietri University of Industry, Tien Kien, PhuTho, Vietnam

Correspondence should be addressed to Thanh-Binh Nguyen; nguyenthanhbinh@hus.edu.vn

Received 2 November 2021; Revised 5 January 2022; Accepted 30 March 2022; Published 26 April 2022

Academic Editor: Dang Quoc Thuyet

Copyright © 2022 Thanh-Binh Nguyen et al. This is an open access article distributed under the Creative Commons Attribution License, which permits unrestricted use, distribution, and reproduction in any medium, provided the original work is properly cited.

A series of composite γ -Fe₂O₃/g-C₃N₄ (denoted as xFeCN with x equal 5, 10, 15, and 20 of γ -Fe₂O₃ percentage in weight) was prepared by calcination and precipitation-impregnation methods. X-ray diffraction (XRD), Fourier transform infrared (FTIR), and X-ray photoelectron spectrometry (XPS) characterizations indicated the successful synthesis of Z-scheme FeCN composites. A red shift of the light absorption region was revealed by UV-vis diffuse reflectance spectroscopy (UV-DRS). In addition, photoluminescence spectroscopy (PL) spectra showed an interface interaction of two phases Fe₂O₃ and g-C₃N₄ in the synthesized composites that improved the charge transfer capacity. The photocatalytic activity of these materials was studied in the photoreduction of CO₂ with H₂O as the reductant in the gaseous phase. The composites exhibited excellent photoactivity compared to undoped g-C₃N₄. The CH₄ production rate over 10FeCN and 15FeCN composites (2.8×10^{-2} and $2.9 \times 10^{-2} \mu\text{mol h}^{-1} \text{g}^{-1}$, respectively) was *ca.* 7 times higher than that over pristine g-C₃N₄ ($0.4 \times 10^{-2} \mu\text{mol h}^{-1} \text{g}^{-1}$). This outstanding photocatalytic property of these composites was explained by the light absorption expansion and the prevention of photogenerated electron-hole pairs recombination due to its Z-scheme structure.

1. Introduction

Carbon dioxide from fossil energy consumption is the most important source of greenhouse gas emissions to the atmosphere, causing global warming [1, 2]. Carbon dioxide capture and storage (CCS) or utilization (CCU) has largely been studied during the last decades [3, 4]. Among them, photocatalytic CO₂ conversion into valuable compounds, such as CH₄ and CH₃OH, is an attractive route [5–7]. Thus, many semiconductors have been investigated as photocatalysts with a particular focus on the development of photocatalytic heterojunction systems by combining various semiconductor materials to form different photocatalyst types such as type I, type II, or especially Z-scheme systems [8–12]. In the type I and type II photocatalysts, there occurs the photogenerated electrons transfer between conduction

bands and holes, one between valance bands of each component in a composite. While in the Z-scheme type, this transfer takes place between the conduction and valance band of two adjacent components. By this characteristic, the Z-scheme photocatalyst has the advantage of mobilizing the potential position of the conduction band or valance band of each semiconductor when they are simultaneously combined for targeted reaction. Thereby, Z-scheme photocatalysts are expected to have stronger redox properties, better charge transfer, and higher improved light absorption yield than those of other simple photocatalyst types.

Recently, graphitic carbon nitride, g-C₃N₄, a semiconductor, has attracted researchers as a potential photocatalyst thanks to its easy synthesis, low cost, and moderate bandgap energy of 2.7 eV, which allows the absorption of visible light [13, 14]. In particular, the conduction band (CB) position of

$g\text{-C}_3\text{N}_4$ is quite negative (-1.14 eV), which is favorable for the photoreduction of CO_2 into almost valuable hydrocarbons such as CH_4 , HCOOH , CH_3OH , and $\text{C}_2\text{H}_5\text{OH}$ [15]. However, one of the major disadvantages of $g\text{-C}_3\text{N}_4$ is the fast electron-hole pair recombination, the relative high bandgap energy to be able to absorb most of the visible light, occupying 44% solar spectra. To improve these drawbacks, one of the strategies is to combine $g\text{-C}_3\text{N}_4$ with other semiconductors [16–20].

Among the semiconductors used as photocatalysts, iron oxide, Fe_2O_3 , is an interesting candidate [21]. One of the outstanding features of this semiconductor is its low synthesis cost and relatively low band gap energy, $E_g = 2.2\text{ eV}$, which allows broad absorption in the visible region of sunlight. Therefore, Fe_2O_3 oxide has been extensively studied as a photocatalyst through the photodegradation of polluted organic compounds in water [22, 23]. However, for the photoreduction of CO_2 , the conduction band potential (CB) is positive ($+1.58\text{ eV}$). So, Fe_2O_3 oxide is not able to reduce this molecule. Combining Fe_2O_3 oxide with another semiconductor having enough negative conduction band potential is required to create an efficient photocatalyst for CO_2 photoreduction [24–29]. The improving photocatalytic activity by adding $\gamma\text{-Fe}_2\text{O}_3$ was also reported in some other works. In the research of Ding et al., for the photoreduction of CO_2 in liquid phase to CH_3OH [30], $a\text{-Fe}_2\text{O}_3/g\text{-C}_3\text{N}_4$ with the weight ratio $a\text{-Fe}_2\text{O}_3: g\text{-C}_3\text{N}_4$ of 60:40 had the best photocatalytic activity with 2.9-fold than pristine $g\text{-C}_3\text{N}_4$. Duan and Mei [31] also reported the highest amount of CH_3OH obtained on 15% $\text{Fe}_2\text{O}_3/g\text{-C}_3\text{N}_4$ (>3.5 fold than pristine $g\text{-C}_3\text{N}_4$). For CO_2 photoreduction in the gas phase, Wong et al. [32] observed the CO formation on dendrite-structured $a\text{-Fe}_2\text{O}_3/g\text{-C}_3\text{N}_4$ ($27.2\ \mu\text{mol h}^{-1}\text{g}^{-1}$), which was about 2.2 times higher than the one on pure $g\text{-C}_3\text{N}_4$ ($10.3\ \mu\text{mol h}^{-1}\text{g}^{-1}$). On the same type of catalyst with urchin-like $a\text{-Fe}_2\text{O}_3$ morphology, Yong Zhou et al. also recognized a CO production rate of $17.8\ \mu\text{mol g}^{-1}\text{h}^{-1}$, 3 times higher than that of pristine $g\text{-C}_3\text{N}_4$ ($6.1\ \mu\text{mol g}^{-1}\text{h}^{-1}$) [33]. Besides, $\text{Fe}_2\text{O}_3/g\text{-C}_3\text{N}_4$ composites also showed higher photoactivity than pure $a\text{-Fe}_2\text{O}_3$ and $g\text{-C}_3\text{N}_4$ in the photodegradation of organic pollutants (Direct Red 81, Rhodamin B, and tetracycline hydrochloride) [34–36]. These studies showed that the morphology of Fe_2O_3 oxide seems to play an important role in the activity of catalyst. The different morphologies may change interface interaction between Fe_2O_3 and $g\text{-C}_3\text{N}_4$ phase, leading to the change in charge carrier, a key factor of photocatalysis.

Based on the analysis above, in this study, we have synthesized Z-scheme $\gamma\text{-Fe}_2\text{O}_3/g\text{-C}_3\text{N}_4$ photocatalysts for CH_4 production from CO_2 photoreduction in the gas phase. This new Z-scheme material could take advantage of the low bandgap energy of $\gamma\text{-Fe}_2\text{O}_3$ oxide and the rather negative conduction band potential of $g\text{-C}_3\text{N}_4$ as well.

2. Experimental

2.1. Materials. Melamine ($\text{C}_3\text{H}_6\text{N}_6$), iron (II) sulfate heptahydrate ($\text{FeSO}_4\cdot 7\text{H}_2\text{O}$), and sodium hydroxide (NaOH) with analytical purity were purchased from

Sigma-Aldrich. Deionized water was used as solvent for all preparations.

2.2. Synthesis of $g\text{-C}_3\text{N}_4$ and $\gamma\text{-Fe}_2\text{O}_3/g\text{-C}_3\text{N}_4$ Composite. Carbon graphitic nitride, $g\text{-C}_3\text{N}_4$, was synthesized by calcination of melamine at 550°C for 3 hours under the nitrogen atmosphere.

A series of $x\%\gamma\text{-Fe}_2\text{O}_3/g\text{-C}_3\text{N}_4$ composites was prepared by the precipitation-impregnation method. First, 1 g of $g\text{-C}_3\text{N}_4$, which were synthesized from melamine calcination, was added in a 100 ml solution of 0.1 M NaOH. The mixture was covered by paraffin paper, stirred, and kept at 60°C for 2 hours. Then, a calculated amount of $\text{FeSO}_4\cdot 7\text{H}_2\text{O}$ was slowly added in the solution above, and the pH was adjusted to 10 with 0.1 M NaOH solution, leading to the formation of a composite material of iron oxide precipitate and $g\text{-C}_3\text{N}_4$. The latter was filtered and washed by deionized water and dried at 70°C . Four Z-scheme $\gamma\text{-Fe}_2\text{O}_3/g\text{-C}_3\text{N}_4$ photocatalysts, denoted as $x\text{FeCN}$, with x equal to 5, 10, 15, or 20 wt.% of $\gamma\text{-Fe}_2\text{O}_3$ were obtained.

2.3. Characterization. All composites were characterized by X-ray diffraction (XRD, model Bruker D8), Fourier transform infrared (FTIR, model 8101M Shimadzu), X-ray photoelectron spectroscopy (XPS, Thermo VG Scientific MultiLab 2000), UV-vis diffuse reflectance spectroscopy (UV-DRS, model Jaco V-530), photoluminescence spectroscopy (PL, model Horiba FluoroMax-4), transmission electron microscopy (TEM, JEM 1400, Plus Jeon), and scanning electron microscopy-energy dispersive X-ray spectrometry (SEM-EDS, Hitachi TM4000 Tabletop Microscope).

2.4. Photocatalytic Procedure. In a typical test, 100 mg of catalyst was added in 15 mL deionized water in a beaker with a 5 cm diameter. The solvent in the mixture was completely evaporated in an oven at 70°C to well disperse the photocatalyst on the bottom of the beaker. After that, the catalyst-containing beaker was placed in a closed stainless reactor equipped with a quartz window (Figure 1). The high purity (99,999%) CO_2 flow of 500 ml/minute bubbled in a closed stainless contains deionized water kept at 25°C before entering the stainless reactor for 30 minutes. Then, a 150W Xenon lamp (Newport model 67005) was switched on for 18 h.

3. Results and Discussion

Figure 2(a) shows the XRD patterns of the fresh $g\text{-C}_3\text{N}_4$ and $x\text{FeCN}$ photocatalysts. The formation of $g\text{-C}_3\text{N}_4$ by melamine calcination was confirmed by the presence of peaks at 2θ of 13.2 and 27.3° (JCPDS 87–1526). For the composite photocatalysts, the characteristic peaks of $\gamma\text{-Fe}_2\text{O}_3$ appeared in all patterns with 2θ at 30.2 , 35.7 , 43.2 , 53.8 , 57.2 , and 62.9° (JCPDS 004–075). The peak intensity of the $\gamma\text{-Fe}_2\text{O}_3$ phase is proportional to its content in the composite materials.

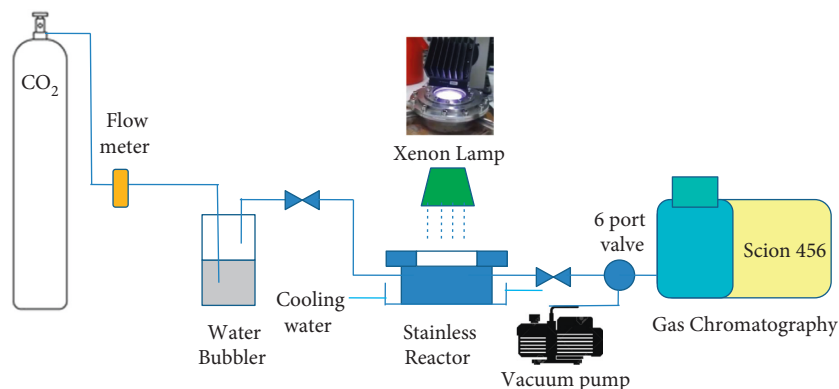


FIGURE 1: Scheme of the photocatalytic reactor used in this work.

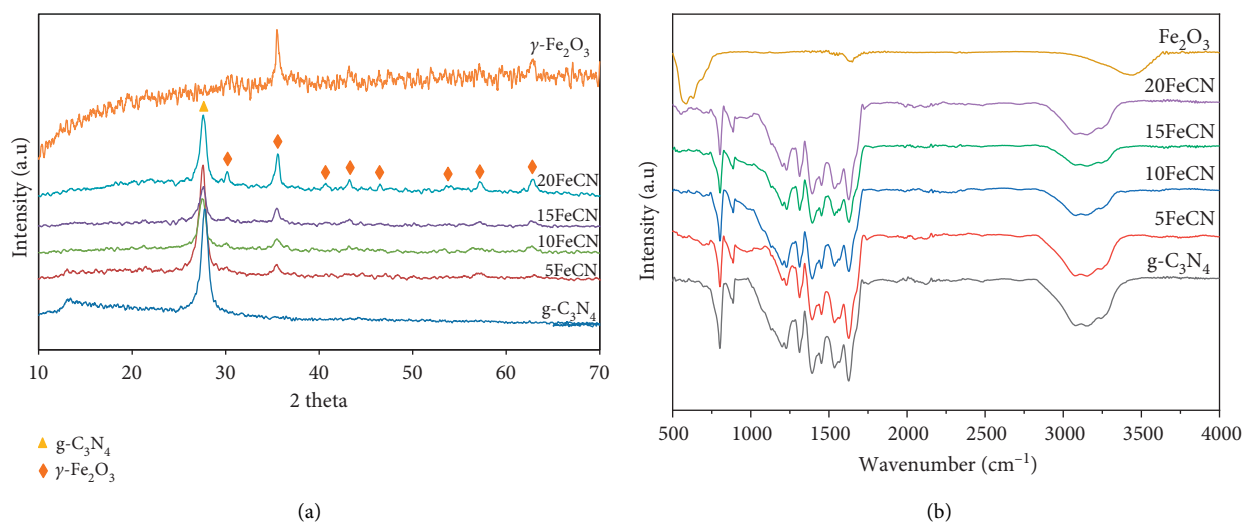
FIGURE 2: XRD patterns (a) and FTIR (b) spectra of $g\text{-C}_3\text{N}_4$, $x\text{FeCN}$ composites.

Figure 2(b) shows the FTIR spectra of all fresh photocatalysts. All these materials have similar characteristic signals of $g\text{-C}_3\text{N}_4$ structure. The peak at 804 and 887 cm^{-1} is attributed to the heptazine stretching mode [37], while those at $1203\text{--}1630\text{ cm}^{-1}$ correspond to stretching vibrations of $\text{C}=\text{N}$ and $\text{C}-\text{N}$ bonds of the heterocycle [38, 39]. For the broad band from 3000 to 3500 cm^{-1} , the signals were ascribed to the vibration of NH_2 and NH functional groups of $g\text{-C}_3\text{N}_4$ and the OH group of adsorbed water [40]. In addition, the weak signals observed at 586 cm^{-1} originated from the $\text{Fe}-\text{O}$ bond vibrations [41]. These results confirmed the formation of the two expected crystalline phases of $g\text{-C}_3\text{N}_4$ and $\gamma\text{-Fe}_2\text{O}_3$ in the photocatalysts synthesized. In order to confirm the formation of composite materials between these two components, XPS analysis was performed for one photocatalyst containing 10 wt% of $\gamma\text{-Fe}_2\text{O}_3$ (Figure 3). The general XPS spectrum (Figure 3(a)) shows the presence of Fe, O, C, and N on the surface of this photocatalyst. On the high-resolution Fe elemental spectrum (Figure 3(b)), there are two major peaks at the binding energy 711.2 and 724.7 eV corresponding to $\text{Fe}^{3+}2p_{3/2}$ and $\text{Fe}^{3+}2p_{1/2}$, respectively. These two peaks are characteristics of the Fe^{3+} oxidation state as observed on the XPS spectrum of Fe_2O_3

oxide [42, 43]. Besides, two satellite peaks can be detected at positions 718.2 and 731.0 eV . With the $\text{C}1s$ spectrum (Figure 3(e)), there are three peaks at 284.9 , 286.5 , and 288.5 eV . The first peak at 284.9 eV is assigned to $\text{C}-\text{C}/\text{C}=\text{C}$ bonds, the second to the carbon of the $\text{C}-\text{NH}_2$ group, and the third to bonded C in the heptazine structure ($\text{N}-\text{C}=\text{N}$) [44, 45]. In the $\text{N}1s$ spectrum (Figure 3(d)), the peak deconvolution shows the presence of 3 peaks at 399.0 , 400.3 , and 401.2 eV , which correspond to Sp^2 bonded N in triazine ring ($\text{C}-\text{N}=\text{C}$), the tertiary nitrogen $\text{N}-(\text{C})_3$ group in the heptazine structure, and N in the $\text{C}-\text{N}-\text{H}$ group, respectively [39, 40]. For the oxygen element (Figure 3(c)), the peak deconvolution of $\text{O}1s$ indicates the existence of three components: lattice oxygen of $\text{Fe}-\text{O}$ bond (529.7 eV), oxygen of surface hydroxyl- OH (531.0 eV), and the one of adsorbed water H_2O (533.3 eV) [43]. Hence, the results of XPS, XRD, and IR proved that $\gamma\text{-Fe}_2\text{O}_3/g\text{-C}_3\text{N}_4$ composites were successfully synthesized.

In order to predict the light absorption ability, all composites and $g\text{-C}_3\text{N}_4$ were measured by the UV-DRS method. Figures 4(a) and 4(b) show the obtained results. From the Kubelka-Munk function, the obtained bandgap energy was of 2.63 , 2.54 , 2.47 , 2.25 , 1.95 , and 1.80 eV for

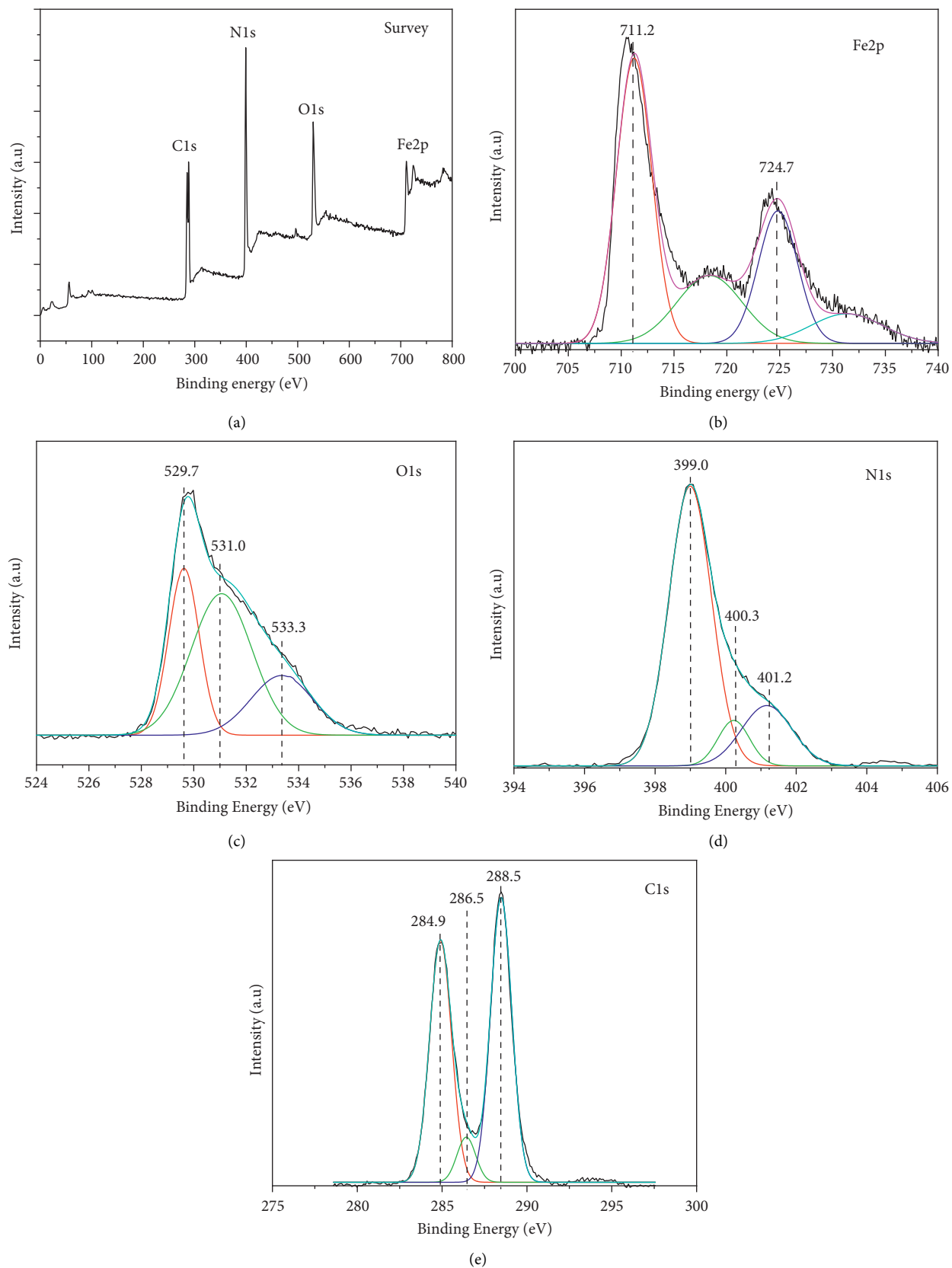


FIGURE 3: XPS survey of 10FeCN composite (a) and its XPS spectra of Fe2p (b), O1s (c), N1s (d), and C1s (e).

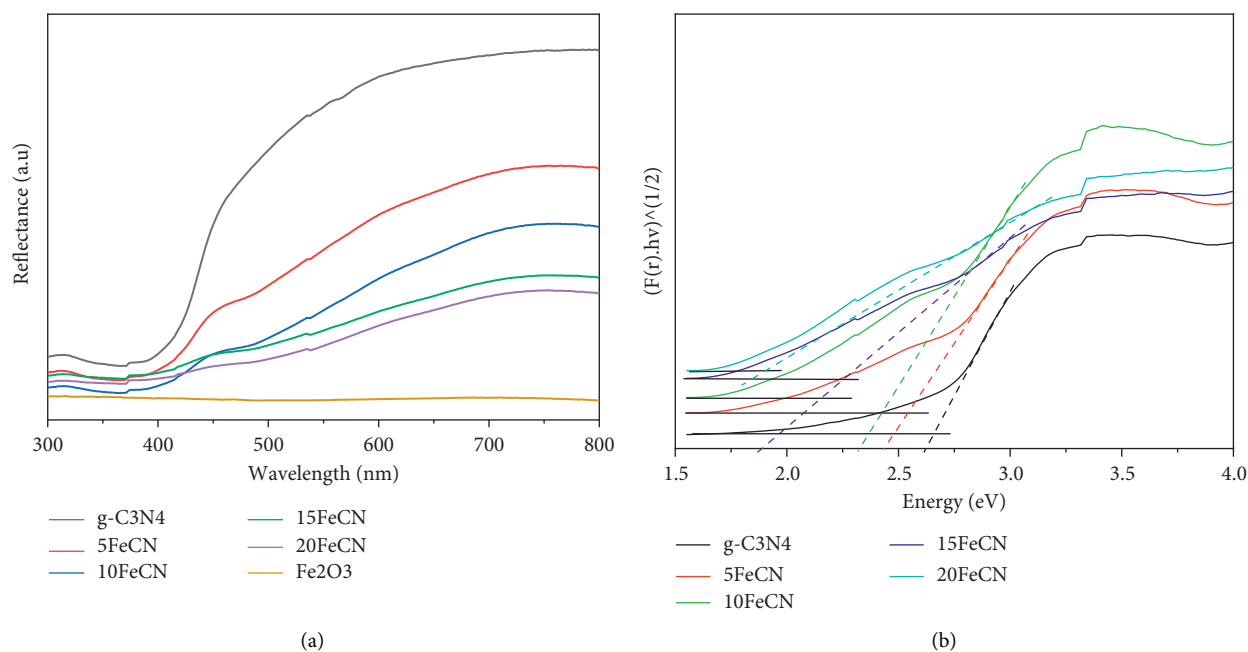


FIGURE 4: UV-DRS spectra (a) and Kubelka–Munk function (b) of xFeCN composites.

g-C₃N₄, 5FeCN, 10FeCN, 15FeCN, 20FeCN, and γ -Fe₂O₃, respectively. So, the increase of γ -Fe₂O₃ content led to decrease of the bandgap energy. In other words, it means that the light absorption region of catalysts shifted more in the visible light wavelength by increasing the γ -Fe₂O₃ content. Hence, the photocatalytic activity of composites is expected to be improved.

To estimate the recombination of electron-hole pair phenomena, the PL spectroscopy was carried out for g-C₃N₄, γ -Fe₂O₃, and 10FeCN composites (Figure 5(a)). As observed, the intensity of PL spectrum of g-C₃N₄ is nearly twice in comparison with the one of 10FeCN. No signal was observed on PL spectra of Fe₂O₃ at activated wavelength. This result reflected that the presence of γ -Fe₂O₃ and its interface interaction with g-C₃N₄ seem to inhibit the photogenerated electron-hole pairs recombination, which could improve photoactivity.

Figures 5(b), 5(c), and 5(d) show the SEM image and different element distribution of the 10FeCN sample. It is obvious that Fe and O elements or Fe₂O₃ phase were quite homogeneously dispersed on the surface of g-C₃N₄. The elemental composition is given in Table 1. It is noted that the experimental composition is quite.

The morphology of composite 10FeCN was characterized by TEM (Figure 6). It is obvious that the particle Fe₂O₃ is in cubic form with average size of 10 nm. Apart from γ -Fe₂O₃ particles dispersed on the g-C₃N₄ surface, it seems that some these particles were covered by g-C₃N₄ layer to form core-shell structure Fe₂O₃@g-C₃N₄.

The photocatalytic activity was evaluated through photoreduction of CO₂. Figure 7(a) shows the obtained results. Methane was the main production of the reaction, while CO was not noticeable. No product was detected on γ -Fe₂O₃. This is explained by the more positive value of its conduction

band potential in comparison of that reduction potential of CO₂/CH₄ (−0.24 V) [2]. It was noted that the presence of γ -Fe₂O₃ remarkably impacted the CH₄ formation. A volcano-like evolution of methane formation as a function of γ -Fe₂O₃ is observed. Concretely, under the same operational conditions, the amount of CH₄ formed is 0.4×10^{-2} , 2.1×10^{-2} , 2.8×10^{-2} , 2.9×10^{-2} , and $1.0 \times 10^{-2} \mu\text{mol g}^{-1} \text{h}^{-1}$ for g-C₃N₄, 5FeCN, 10FeCN, 15FeCN, and 20FeCN, respectively. Hence, the maximum CH₄ formation quickly increased when rising the γ -Fe₂O₃ content and reached the maximum with 10FeCN and 15FeCN composites. Thus, compared to pristine g-C₃N₄, the produced amount of CH₄ over 10FeCN and 15FeCN composites was 7 fold. However, at higher γ -Fe₂O₃ content, e.g., 20wt.% Fe₂O₃, CH₄ production dropped rapidly to $1.0 \times 10^{-2} \mu\text{mol g}^{-1} \text{h}^{-1}$. In comparison with the research on urchin-like Fe₂O₃/g-C₃N₄ and dendrite-structured Fe₂O₃/g-C₃N₄ catalysts for CO₂ photoreduction in the gas phase, CH₄ gas was the preferred product on this catalyst, instead of CO [32, 33]. Hence, the obtained results show interesting photocatalytic activity of the synthesized composite materials and also prove the good combination of two phases, γ -Fe₂O₃ and g-C₃N₄, to make new active photocatalysts. The small formed CH₄ amount was probably due to the low power of xenon lamp (only 150W). To justify these results, a blank test (without catalyst) and a test on g-C₃N₄ under N₂ gas were carried out. No CH₄ amount was detected for these ones. In addition, the test was performed also on the mixture of 10% (wt) of γ -Fe₂O₃ with g-C₃N₄ (Figure 7(a)), and the CH₄ product is under detectable limit that could be evidence for the absence of phase interaction between γ -Fe₂O₃ and g-C₃N₄ as well as the presence of γ -Fe₂O₃ hindering the illumination on g-C₃N₄.

Generally, the outstanding photoactivity of γ -Fe₂O₃/g-C₃N₄ composite materials compared to g-C₃N₄ is assigned to

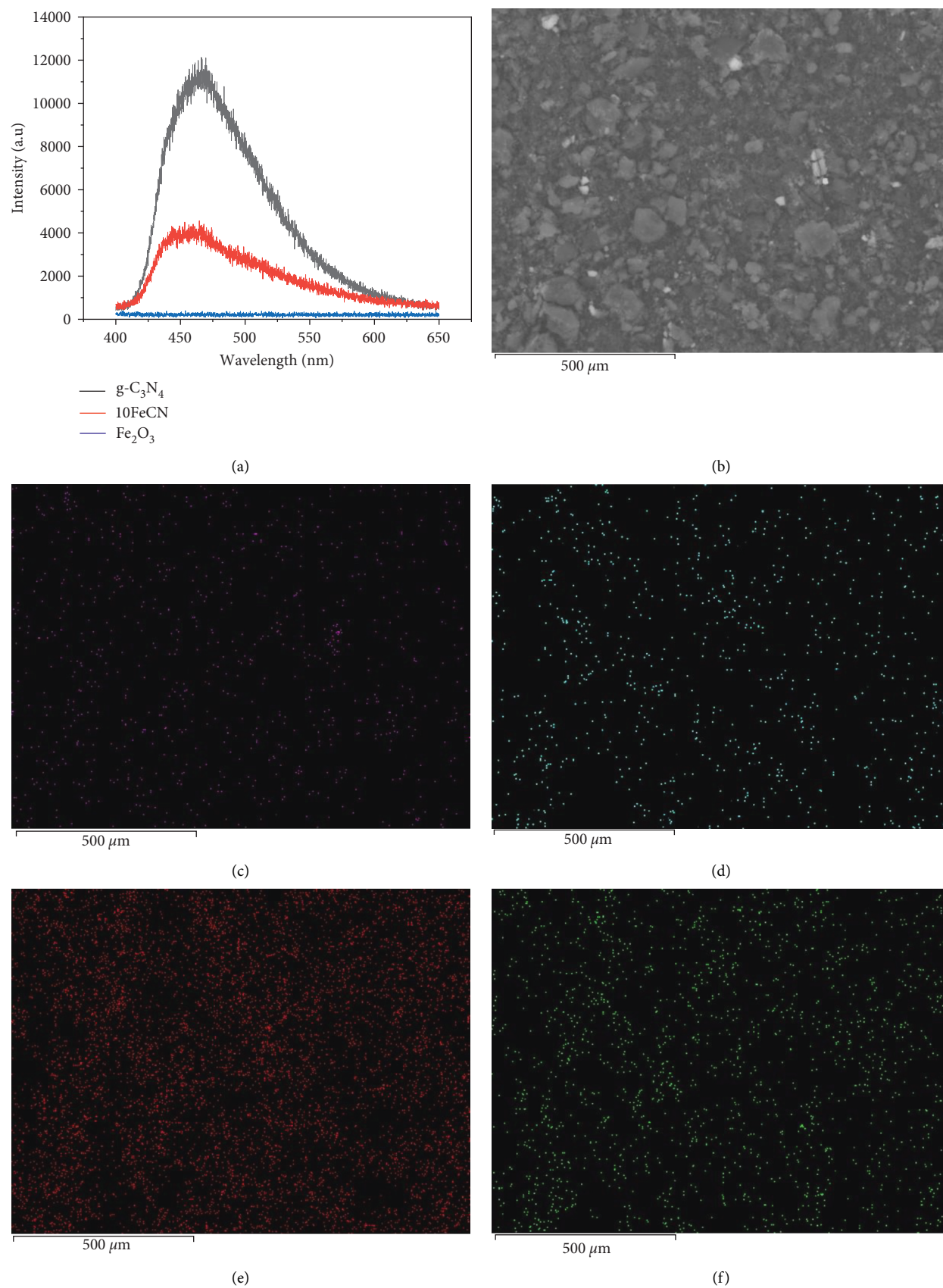


FIGURE 5: PL spectra of $g\text{-C}_3\text{N}_4$, $\gamma\text{-Fe}_2\text{O}_3$, and 10FeCN composite. (a) SEM mapping images of different elements in 10FeCN : SEM image (b), Fe distribution (c), O distribution (d), C distribution (e), and N distribution (f).

TABLE 1: Weight percentages of different elements in the composition of 10FeCN.

Element	Theoretical percent	Experimental percent
Fe	6.99	7.26
O	3.01	3.24
C	35.22	36.57
N	54.78	52.93

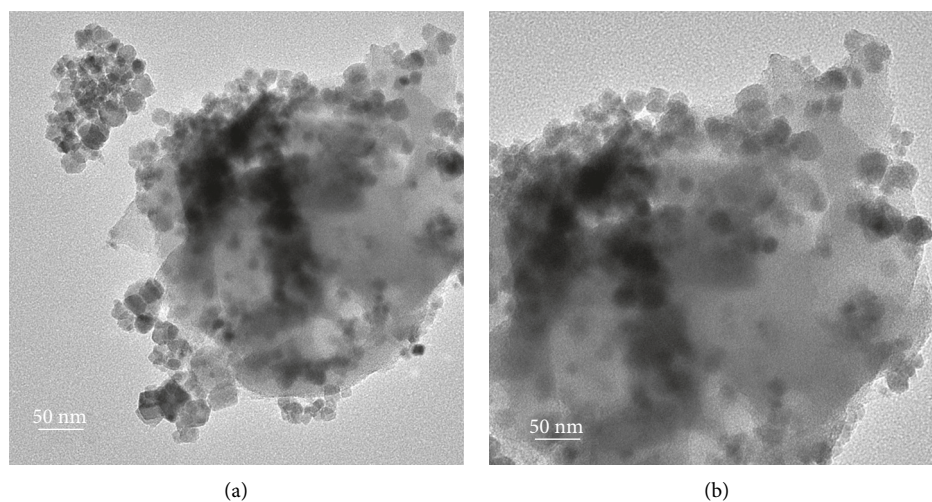
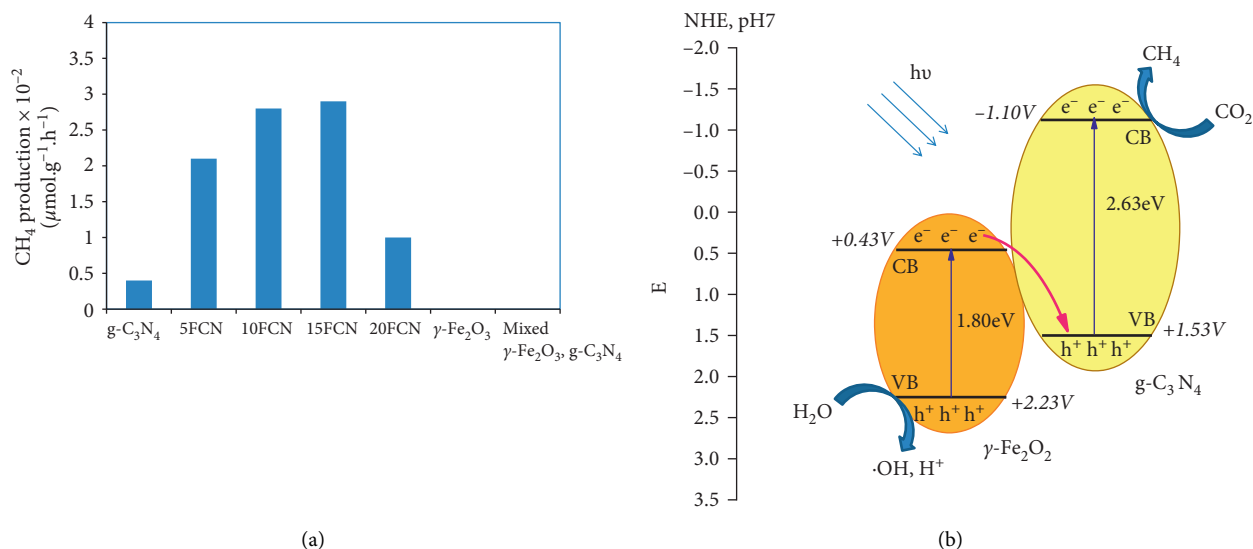


FIGURE 6: TEM images of 10FeCN.

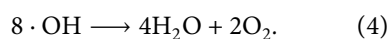
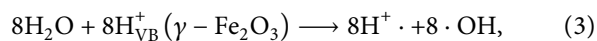
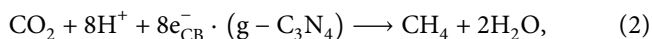
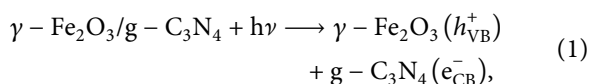
FIGURE 7: CH₄ production on g-C₃N₄ and different xFeCN composites (a); proposed mechanism of CO₂ photoreduction on Z-scheme structure of γ-Fe₂O₃/g-C₃N₄ (b).

better light-harvesting ability and charge transfer than those of single phase of γ-Fe₂O₃ or g-C₃N₄. It should be emphasized that the charge transfer process in the Z-scheme structure not only reduces photoelectron-hole pair recombination but also makes photocatalyst, the redox potential, stronger: CB potential more negative and VB potential more positive. In addition, it seems that the quite small size

particles of γ-Fe₂O₃ as observed in TEM images, about 10 nm of diameter, have improved the interface interaction of composite γ-Fe₂O₃/g-C₃N₄. The increase of γ-Fe₂O₃ quantity superior of 15% (wt) has led to the decrease of photoactivity. This is probably due to the strong sintering of γ-Fe₂O₃ nanoparticles, causing less interface interaction. Besides, the accumulation of γ-Fe₂O₃ nanoparticles could

cover g-C₃N₄ surface and inhibits the irradiation on this phase. Hence, the γ -Fe₂O₃ quantity of 10% (wt) was the most suitable to obtain the highest photoactivity.

From UV-DRS spectrum and Mulliken electronegativity theory, the valance band (VB) and conduction band (CB) of γ -Fe₂O₃ and g-C₃N₄ were calculated [30]. According to this theory, $E_{CB} = X - E_c - 0.5E_g$, where E_{CB} is the conduction band edge energy, X is the electronegativity of the semiconductor (equal 5.825 eV for Fe₂O₃ and 4.72 eV for g-C₃N₄), E_c , equal 4.5 eV, is the energy of free electrons with hydrogen scale, and E_g is the bandgap energy of semiconductor. Basing on this equation and concrete value of each parameter, it is found that VB and CB of γ -Fe₂O₃ and g-C₃N₄ are +2.23, +0.43 eV and +1.53, -1.10 eV, respectively. Figure 7(b) shows a possible photoreduction mechanism of CO₂ photoreduction into CH₄. According to this Z-scheme composite, all the two phases, γ -Fe₂O₃ and g-C₃N₄, harvested the irradiated light and generated electron-hole pairs. The photogenerated electron located on CB of γ -Fe₂O₃ migrated and recombined with photogenerated holes located on the valance band (VB) of g-C₃N₄. This process allows broadening the light absorption region and also prevents recombination of photogenerated electron-hole pairs that both improved the photocatalytic activity. The details of this process are presented through the following equations:



4. Conclusions

In this work, different Z-scheme photocatalysts, γ -Fe₂O₃/g-C₃N₄, were synthesized by simple methods of calcination and impregnation-precipitation. XRD, IR, and XPS characterizations of these materials confirmed the formation of composite structure of these photocatalysts, wherein γ -Fe₂O₃ grew on g-C₃N₄ surface. SEM analysis highlighted a good distribution of Fe on the surface of g-C₃N₄ support. The UV-DRS and PL spectra of the photocatalyst containing 10 wt.% γ -Fe₂O₃ evidenced interface interaction of the two phases of γ -Fe₂O₃ and g-C₃N₄.

The catalytic performance of these materials was evaluated through the CO₂ photoreduction in the gaseous phase. Methane was found as the main product, while no trace of CO was observed. According to CH₄ production, the photocatalytic activity followed the following order: 15FCN ($2.9 \times 10^{-2} \mu\text{mol g}^{-1} \text{h}^{-1}$) > 10FeCN ($2.8 \times 10^{-2} \mu\text{mol g}^{-1} \text{h}^{-1}$) > 5FeCN ($2.1 \times 10^{-2} \mu\text{mol g}^{-1} \text{h}^{-1}$) > 20FeCN ($1.0 \times 10^{-2} \mu\text{mol g}^{-1} \text{h}^{-1}$) > g-C₃N₄ ($0.4 \times 10^{-2} \mu\text{mol g}^{-1} \text{h}^{-1}$). Hence, 10FeCN and 15FeCN composites had the highest photoactivity, which is approximately 7 times higher than that on bulk g-C₃N₄. This could be explained by a synergy

combination and interaction of the two phases γ -Fe₂O₃ and g-C₃N₄, leading to the Z-scheme structure composites, which improved light absorption with red-shift light and also diminishes photogenerated electron-hole pairs recombination. These outstanding results are promising for the design of a low-cost and highly efficient photocatalyst for CO₂ reduction on the basis of γ -Fe₂O₃ and g-C₃N₄.

Data Availability

The data used to support the findings of this study are included within the article.

Conflicts of Interest

The authors declare that there are no conflicts of interest.

Acknowledgments

This research was funded by the Vietnam National Foundation for Science and Technology Development (NAFOSTED) under grant no. 104.05-2017.39.\S1HCIFS01\DEMDData\16955\MYFILE-S\HINDAWI\JAMC\1358437\PROOF\PREEDITING\gs1.

References

- [1] L. Jing, W. Zhou, G. Tian, and H. Fu, "Surface tuning for oxide-based nanomaterials as efficient photocatalysts," *Chemical Society Reviews*, vol. 42, no. 24, pp. 9509–9549, 2013.
- [2] L. Yuan and Y.-J. Xu, "Photocatalytic conversion of CO₂ into value-added and renewable fuels," *Applied Surface Science*, vol. 342, pp. 154–167, 2015.
- [3] J. He and C. Janáky, "Recent advances in solar-driven carbon dioxide conversion: expectations versus reality," *ACS Energy Letters*, vol. 5, no. 6, pp. 1996–2014, 2020.
- [4] F. Nocito and A. Dibenedetto, "Atmospheric CO₂ mitigation technologies: carbon capture utilization and storage," *Current Opinion in Green and Sustainable Chemistry*, vol. 21, pp. 34–43, 2020.
- [5] A. Olivo, V. Trevisan, E. Ghedini et al., "CO₂ photoreduction with water: catalyst and process investigation," *Journal of CO₂ Utilization*, vol. 12, pp. 86–94, 2015.
- [6] L. Liu, S. Wang, H. Huang, Y. Zhang, and T. Ma, "Surface sites engineering on semiconductors to boost photocatalytic CO₂ reduction," *Nano Energy*, vol. 75, Article ID 104959, 2020.
- [7] S. Matavos-Aramyan, S. Soukhakian, M. H. Jazebizadeh et al., "On engineering strategies for photoselective CO₂ reduction - a thorough review," *Applied Materials Today*, vol. 18, Article ID 100499, 2020.
- [8] X. Quanlong, Z. Liuyang, Y. Jianguo, G. A. Al, and J. Mietek, "Direct Z-scheme photocatalysts: Principles, synthesis, and applications," *Materialstoday*, vol. 21, no. 10, pp. 1042–1063, 2018.
- [9] G. Zhang, Z. Wang, and J. Wu, "Construction of a Z-scheme heterojunction for high-efficiency visible-light-driven photocatalytic CO₂ reduction," *Nanoscale*, vol. 13, no. 8, pp. 4359–4389, 2021.
- [10] X. Dai, L. Chen, Z. Li et al., "CuS/KTa_{0.75}Nb_{0.25}O₃ nanocomposite utilizing solar and mechanical energy for catalytic N₂ fixation," *Journal of Colloid and Interface Science*, vol. 603, pp. 220–232, 2021.

- [11] Lu Chen, W. Zhang, J. Wang et al., *High Piezo/photocatalytic Efficiency of Ag/Bi5O7I Nanocomposite Using Mechanical and Solar Energy for N₂ Fixation and Methyl Orange Degradation*, Green Energy & Environment, in press, 2021.
- [12] L. Chen, X. Dai, X. Li et al., "A novel Bi₂S₃/KTa_{0.75}Nb_{0.25}O₃ nanocomposite with high efficiency for photocatalytic and piezocatalytic N₂ fixation," *Journal of Materials Chemistry*, vol. 9, pp. 13344–13354, 2021.
- [13] J. Zhu, P. Xiao, H. Li, and S. A. C. Carabineiro, "Graphitic carbon nitride: synthesis, properties, and applications in catalysis," *ACS Applied Materials & Interfaces*, vol. 6, no. 19, pp. 16449–16465, 2014.
- [14] Z. Zhao, Y. Sun, and F. Dong, "Graphitic carbon nitride based nanocomposites: a review," *Nanoscale*, vol. 7, no. 1, pp. 15–37, 2015.
- [15] L. Wang, K. Wang, T. He, Y. Zhao, H. Song, and H. Wang, "Graphitic carbon nitride-based photocatalytic materials: preparation strategy and application," *ACS Sustainable Chemistry & Engineering*, vol. 8, no. 43, pp. 16048–16085, 2020.
- [16] U. Ghosh and A. Pal, "Graphitic carbon nitride based Z scheme photocatalysts: design considerations, synthesis, characterization and applications," *Journal of Industrial and Engineering Chemistry*, vol. 79, pp. 383–408, 2019.
- [17] J. Lin, W. Tian, H. Zhang, X. Duan, H. Sun, and S. Wang, "Graphitic carbon nitride-based Z-scheme structure for photocatalytic CO₂ reduction," *Energy and Fuels*, vol. 35, no. 1, pp. 7–24, 2021, 7–24.
- [18] Yiming He, Yan Wang, Lihong Zhang, and Botao Teng, "Maohong Fan, High-efficiency conversion of CO₂ to fuel over ZnO/g-C₃N₄ photocatalyst," *Appl. Catal. B: Environ*, vol. 168–169, pp. 1–8, 2015.
- [19] Y. He, L. Zhang, M. Fan et al., "Z-scheme SnO₂-x/g-C₃N₄ composite as an efficient photocatalyst for dye degradation and photocatalytic CO₂ reduction/x/g-C₃N₄ composite as an efficient photocatalyst for dye degradation and photocatalytic CO₂ reduction," *Solar Energy Materials and Solar Cells*, vol. 137, pp. 175–184, 2015.
- [20] Y. He, L. Zhang, B. Teng, and M. Fan, "New application of Z-scheme Ag₃PO₄/g-C₃N₄ composite in converting CO₂ to fuel," *Environmental Science and Technology*, vol. 49, no. 1, pp. 649–656, 2015.
- [21] M. Mishra and D.-M. Chun, "α-Fe₂O₃ as a photocatalytic material: a review," *Applied Catalysis A: General*, vol. 498, pp. 126–141, 2015.
- [22] C.N.C Hitam and A.A Jalil, "A review on exploration of Fe₂O₃ photocatalyst towards degradation of dyes and organic contaminants," *J. Environ. Manage*, vol. 258, Article ID 110050, 2020.
- [23] A. H. Asif, S. Wang, and H. Sun, "Hematite-based nano-materials for photocatalytic degradation of pharmaceuticals and personal care products (PPCPs): a short review," *Current Opinion in Green and Sustainable Chemistry*, vol. 28, Article ID 100447, 2021.
- [24] J.-C. Wang, L. Zhang, W.-X. Fang et al., "Enhanced photo-reduction CO₂ activity over direct Z-scheme α-Fe₂O₃/Cu₂O heterostructures under visible light irradiation," *ACS Applied Materials & Interfaces*, vol. 7, no. 16, pp. 8631–8639, 2015.
- [25] J. Song, Y. Lu, Y. Lin, Q. Liu, X. Wang, and W. Su, "A direct Z-scheme α-Fe₂O₃/LaTiO₂N visible-light photocatalyst for enhanced CO₂ reduction activity," *Applied Catalysis B: Environmental*, vol. 292, Article ID 120185, 2021.
- [26] Y. Jia, W. Zhang, J. Yeon Do, M. Kang, and C. Liu, "Z scheme SnFe₂O₄/α-Fe₂O₃ micro-octahedron with intimated interface for photocatalytic CO₂ reduction," *Chemical Engineering Journal*, vol. 402, Article ID 126193, 2020.
- [27] X. Wang, Q. Li, C. Zhou, Z. Cao, and R. Zhang, "ZnO rod/reduced graphene oxide sensitized by α-Fe₂O₃ nanoparticles for effective visible-light photoreduction of CO₂," *Journal of Colloid and Interface Science*, vol. 554, pp. 335–343, 2019.
- [28] Z. Zhao, C. Shi, Q. Shen et al., "Hierarchical Z-scheme Fe₂O₃@ZnIn₂S₄ core-shell heterostructures with enhanced adsorption capacity enabling significantly improved photocatalytic CO₂ reduction," *CrystEngComm*, vol. 22, no. 47, pp. 8221–8227, 2020.
- [29] A. Kumar, P. K. Prajapati, U. Pal, and S. L. Jain, "Ternary rGO/InVO₄/Fe₂O₃ Z-scheme heterostructured photocatalyst for CO₂ reduction under visible light irradiation," *ACS Sustainable Chemistry & Engineering*, vol. 6, no. 7, pp. 8201–8211, 2018.
- [30] H. Guo, M. Chen, Q. Zhong, Y. Wang, W. Ma, and J. Ding, "Synthesis of Z-scheme α-Fe₂O₃/g-C₃N₄ composite with enhanced visible-light photocatalytic reduction of CO₂ to CH₃OH," *Journal of CO₂ Utilization*, vol. 33, pp. 233–241, 2019.
- [31] B. Duan and L. Mei, "A Z-scheme Fe₂O₃/g-C₃N₄ heterojunction for carbon dioxide to hydrocarbon fuel under visible illuminance," *Journal of Colloid and Interface Science*, vol. 575, pp. 265–273, 2020.
- [32] Z. Jiang, W. Wan, H. Li, S. Yuan, H. Zhao, and P. K. Wong, "A hierarchical Z-scheme α-Fe₂O₃/g-C₃N₄ hybrid for enhanced photocatalytic CO₂ reduction," *Advanced Materials*, vol. 30, no. 10, Article ID 1706108, 2018.
- [33] Y. Shen, Q. Han, J. Hu et al., "Artificial trees for artificial photosynthesis: construction of dendrite-structured α-Fe₂O₃/g-C₃N₄ Z-scheme system for efficient CO₂ reduction into solar fuels," *ACS Applied Energy Materials*, vol. 3, no. 7, pp. 6561–6572, 2020.
- [34] J. Theerthagiri, R. A. Senthil, A. Priya, J. Madhavan, R. J. V. Michael, and Muthupandian Ashokkumar, "Photocatalytic and photoelectronchemical studies of visible-light active α-Fe₂O₃-g-C₃N₄ nanocomposites," *RSC Advances*, vol. 4, pp. 38222–38229, 2014.
- [35] Z. Wang, Y. Fan, R. Wu et al., "Novel magnetic g-C₃N₄/α-Fe₂O₃/Fe₃O₄ composite for the very effective visible-light-Fenton degradation of Orange II," *RSC Advances*, vol. 8, no. 10, pp. 5180–5188, 2018.
- [36] C. Li, S. Yu, H. Che et al., "Fabrication of Z-scheme heterojunction by anchoring mesoporous γ-Fe₂O₃ nanospheres on g-C₃N₄ for degrading tetracycline hydrochloride in water," *ACS Sustainable Chemistry & Engineering*, vol. 6, no. 12, pp. 16437–16447, 2018.
- [37] L. Liu, D. Ma, H. Zheng, X. Li, M. Cheng, and X. Bao, "Synthesis and characterization of microporous carbon nitride," *Microporous and Mesoporous Materials*, vol. 110, no. 2–3, pp. 216–222, 2008.
- [38] X. Wang, K. Maeda, A. Thomas et al., "A metal-free polymeric photocatalyst for hydrogen production from water under visible light," *Nature Materials*, vol. 8, no. 1, pp. 76–80, 2009.
- [39] H. Xu, J. Yan, X. She et al., "Graphene-analogue carbon nitride: novel exfoliation synthesis and its application in photocatalysis and photoelectrochemical selective detection of trace amount of Cu²⁺," *Nanoscale*, vol. 6, no. 3, pp. 1406–1415, 2014.
- [40] F. Yang, V. Kuznetsov, M. Lublow et al., "Solar hydrogen evolution using metal-free photocatalytic polymeric carbon nitride/CuInS₂ composites as photocathodes," *Journal of Materials Chemistry*, vol. 1, pp. 6407–6415, 2013.

- [41] C. Hao, F. Feng, X. Wang et al., "The preparation of Fe₂O₃ nanoparticles by liquid phase-based ultrasonic-assisted method and its application as enzyme-free sensor for the detection of H₂O₂," *RSC Advances*, vol. 5, no. 27, pp. 21161–21169, 2015.
- [42] X.-F. Lu, X.-Y. Chen, W. Zhou, Y.-X. Tong, and G. R. Li, "α-Fe₂O₃@PANI core-shell nanowire arrays as negative electrodes for asymmetric supercapacitors," *ACS Applied Materials & Interfaces*, vol. 7, no. 27, pp. 14843–14850, 2015.
- [43] X. Shi, X. Li, G. Liu et al., "NaCl-assisted synthesis of Fe²⁺-self-doped Fe₂O₃/C₃N₄ nanosheets as efficient Fenton catalyst," *Journal of Materials Science*, vol. 55, no. 23, pp. 10035–10046, 2020.
- [44] C. Ji, S.-N. Yin, S. Sun, and S. Yang, "An in situ mediator-free route to fabricate Cu₂O/g-C₃N₄ type-II heterojunctions for enhanced visible-light photocatalytic H₂ generation, Cong Ji, Su-Na Yin, Shasha Sun, Shengyang Yang," *Applied Surface Science*, vol. 434, pp. 1224–1231, 2018.
- [45] L. Tan, J. Xu, X. Zhang, Z. Hang, Y. Jia, and S. Wang, "Synthesis of g-C₃N₄/CeO₂ nanocomposites with improved catalytic activity on the thermal decomposition of ammonium perchlorate," *Applied Surface Science*, vol. 356, pp. 447–453, 2015.